

## The kinematics of falling maple seeds and the initial transition to a helical motion

This article has been downloaded from IOPscience. Please scroll down to see the full text article.

2012 Nonlinearity 25 C1

(<http://iopscience.iop.org/0951-7715/25/1/C1>)

View [the table of contents for this issue](#), or go to the [journal homepage](#) for more

Download details:

IP Address: 128.253.99.93

The article was downloaded on 11/01/2012 at 03:34

Please note that [terms and conditions apply](#).

# The kinematics of falling maple seeds and the initial transition to a helical motion

Kapil Varshney<sup>1</sup>, Song Chang<sup>2</sup> and Z Jane Wang<sup>1,3</sup>

<sup>1</sup> Sibley School of Mechanical and Aerospace of Engineering, Cornell University, Ithaca, NY 14853, USA

<sup>2</sup> School of Applied and Engineering Physics, Cornell University, Ithaca, NY 14853, USA

<sup>3</sup> Department of Physics, Cornell University, Ithaca, NY 14853, USA

E-mail: [jane.wang@cornell.edu](mailto:jane.wang@cornell.edu)

Received 22 November 2011

Published 15 December 2011

Online at [stacks.iop.org/Non/25/C1](http://stacks.iop.org/Non/25/C1)

## Abstract

A maple seed falls in a characteristic helical motion. A crude analogy with autorotation of a wind turbine suggests that the torque due to the aerodynamic force would initiate the gyration of the seed. We were therefore surprised that a seed with a torn wing gyrates in a similar manner as a full-winged seed. In fact, a seed with only a sliver of leading edge can still gyrate. Thus the gyrating motion appears not to fully depend on the aerodynamic force. If, on the other hand, the aerodynamic force is completely absent, a seed would fall from rest like a rock in a vacuum.

To investigate how the seed reaches its steady helical motion, we use a high-speed digital camera to film the intact and cut seeds at 1000 Hz. With a mirror, the camera records two views simultaneously so that we can extract the 3D kinematics of the wing. We tracked the centre of mass and quantified the descending speed, the azimuthal rotation, and the cone angle for seeds with wings of different shapes. We found that the initial transition from rest to a steady gyration occurs in three steps: a tumble about the span-wise direction, followed by a tilt towards the vertical axis, leading to the gyration about the vertical axis and an opening of the cone angle before settling into a steady state. We offer a new explanation for the cause of the auto-gyration that accounts for these three stages.

Mathematics Subject Classification: 76Z99, 70B10, 92B99

(Some figures may appear in colour only in the online journal)

## 1. Introduction

The maple samara (winged-seed) auto-gyrates as it falls. The spiral motion appears to be stable against wind disturbance and is insensitive to the initial conditions. The auto-gyration is a characteristic of many long-dispersal tree seeds [1]. As the samara glides along a helical path,

it generates an aerodynamic force that slows down its descent. The slower descent leads to a longer dispersion under the wind condition, advantageous for the propagation of its species. Field studies and statistical analyses of tree seeds have correlated the descent speed and the dispersal range [1–8]. Laboratory studies have also applied aerodynamic force models to describe the speed of descent and the cone angles [4, 9, 10]. Recent experimental studies have further quantified the aerodynamic flow structure around dynamically scaled mechanical seeds immersed in a viscous fluid showing the role of the leading-edge vortex on the aerodynamic forces [11]. The falling kinematics of the seed, on the other hand, has not yet been quantified, apart from qualitative descriptions [4, 9, 12].

A main puzzle for us was to understand exactly how the seed settles into its steady descent. At first sight, the gyrating motion seems to be closely related to the autorotation of a wind turbine. The lift on the wing due to the falling velocity of the seed exerts a torque to spin the seed about the vertical axis. Rotation of this kind falls into the broad category of rotational phenomena resulting from fluid and solid interactions. The autorotation was studied in the context of a wing free to rotate about its fixed axis [13–16]. A more general class of phenomena includes free-falling objects in a fluid. A falling object in a fluid exhibits a rich dynamical behaviour, such as fluttering (oscillation from side to side), tumbling (continuous rotation) and chaotic motions [17–30]. Maxwell [17] was among the first to attempt to explain the steady tumbling motion qualitatively. In recent literature, there have been extensive experimental studies in fluid dynamics literature that quantified the phase diagram for plates falling in a fluid [15, 20, 23, 25]. The falling dynamics depends critically on the moment of inertia as well as on the Reynolds number. These rich dynamics have also attracted the attention of those who are interested in dynamical systems [22, 24, 26]. The transition among different dynamical states in 2D can be partially explained by the nature of the two fixed points in the system, which is characterized by a Hopf and a Shnikov bifurcation, respectively [26]. All of these motions, the tumbling, the flutter and the mixture of the two, have been observed in tree seeds [1].

A surprise came when we cut off much of the wing of a maple seed and found that the seed still gyrated about the vertical axis. This immediately suggests that the cause of the gyration has little to do with the steady-state aerodynamic torque on a full winged-seed. In what follows, we report detailed measurements of the kinematics of falling seeds with intact and cut wings. By examining the transitional state, we offer a new explanation for the cause of auto-gyration.

## 2. Experimental apparatus and measurement procedure

To capture time dependence in seed motions with six degrees of freedom, top and side views of the free-falling maple seeds were recorded using a single high-speed camera. Figure 1 shows the experimental set-up and arrangements of the apparatus which comprises a high-speed camera (Vision Research, Phantom v5.0), a mirror of size 30 cm  $\times$  45 cm which was mounted at 45° from horizontal, and two white backgrounds of which one was placed on the opposite side of the mirror and the other was placed horizontally at 1.5 m above the mirror. Both backgrounds were illuminated homogeneously to obtain good contrast.

A calibration has been performed to find the instantaneous size of the seed because image size of the falling seed is a function of the distance between the seed and the lens. Two calibrations one for side view and one for top view have been performed. An orthogonal grid of 1 cm  $\times$  1 cm square lines was plotted on a sheet of paper. For the top view, the sheet was positioned horizontally and moved up in the Z-axis to ten known distances, 16 cm in total, from the top edge of the mirror. For the side view, the sheet was positioned vertically and then moved only horizontally towards the camera to three known distances, 15 cm in total. It

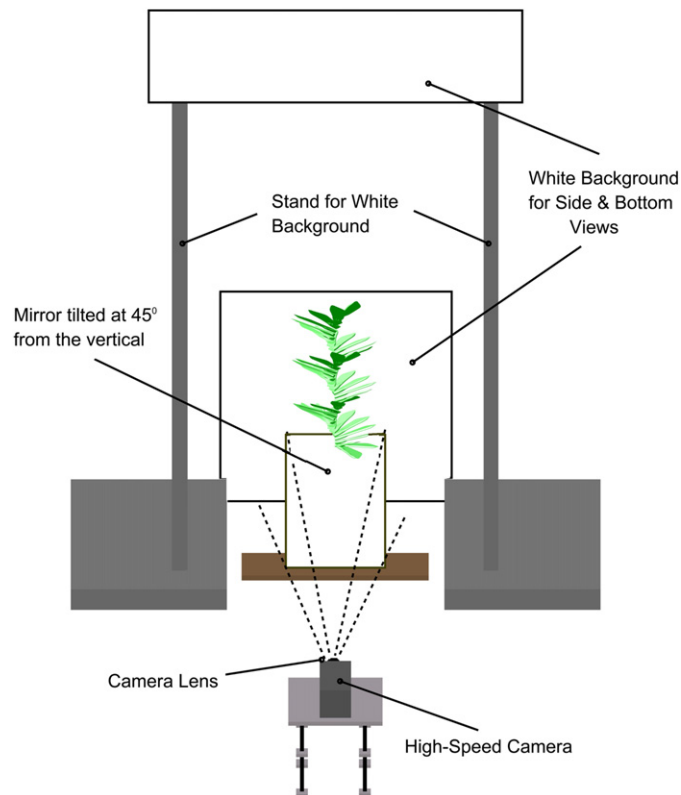


**Figure 1.** The experimental apparatus; the mirror, maple seed and the high-speed digital video camera shown schematically.











should be noted that the seeds were dropped in such a way that they fell on the mirror within the calibration area. For side and top views, we only considered the images in which the seed was above the top edge of the mirror.

We collected maple seeds in Ithaca, NY region in 2011, and performed two series of experiments on altered maple seeds in addition to their natural forms. One is to cut the wing in five steps, and the other is to cut the nut in three steps, progressively. In each experiment, we selected ten seeds, and we filmed the seed motion after each cut three times. Table 1 shows images of the seeds, their masses, and areas after each cut. The maple seeds were dropped in still air with their long axis horizontal and acute axis vertical from a height of approximately 1.5 m and trajectories of the falling seeds were recorded at 1000 fps. The frame rate was sufficient to resolve both the translational and the rotational motion during all parts of the descent. All the experiments were performed in a closed laboratory to prevent any unwanted airflow. All seeds were coloured black homogeneously so that in each frame we can observe the dark seed image on the white background.

### 3. Three-dimensional seed kinematics

The seed exhibits remarkable stability during its fall. A random toss always leads to the steady-state gyration. In the steady state, the seed rotates about the vertical axis with the leading-edge cutting the flow. Viewed from the top, it can rotate either in a clockwise or counter-clockwise

**Table 1.** Free-flight parameters of free-falling seeds in steady state after removing wing as well as nut gradually.

Cut	Mass (mg)	Area (mm <sup>2</sup> )	$ V_z $ (m/s)	$\omega_\phi$ (rad/s)	Cone angle (°)
<u>Wing Cut</u>					
(0) 	170.6	612.8	0.94	77.9	64.2
(1) 	166.1	503.6	1.04	86.9	68.2
(2) 	158.6	344.8	1.00	134.7	71.5
(3) 	154.2	287.4	1.11	173.7	72.9
(4) 	149.4	202.0	2.95	124.5	73.6
(5) 	146.4	191.6	4.30	66.1	53.4
<u>Nut Cut</u>					
(0) 	195.8	546.1	1.18	82.7	71.2
(1) 	162.9	528.5	0.92	79.3	71.8
(2) 	127.4	504.1	0.96	71.4	69.7
(3) 	92.2	486.9	0.88	68.8	72.3

direction, thus can have either left or right chirality. The wing is tilted down towards the nut and thus the wing tip traces out a cone relative to the root. The tilt and the pitch of the wing remain largely constant, and to the first approximation, the wing falls along a helical path. A helix is nothing but a straight line along a cylinder. The wing follows a simple gliding motion along a helix with an almost constant angle of attack.

Unexpectedly, almost all cut seeds, some with barely any wing left, also reach a steady gyration motion. Figure 2 shows the trajectories of a full and a cut seed. Apart from the expected large falling speed, the cut seed falls in much the same way as the full seed, even the cone angles are similar.

To quantify the kinematics, we systematically cut the seeds along the span and the chord directions, and filmed and extracted their kinematics. During the fall the seed remained rigid. Its kinematics are fully characterized by the position of centre of mass and three Euler angles. They can be deduced from the two views of the seed, a side ( $XZ$ ) view directly observed by the camera, and a bottom ( $XY$ ) view reflected by the mirror. The  $X$ ,  $Y$  and  $Z$  are the lab coordinates which correspond to the horizontal right, horizontally away from the camera, and vertically upwards, respectively. The  $x$ ,  $y$  and  $z$  are the wing frame coordinates which correspond to the span-wise direction, the chord direction and the normal to the wing (see figure 3). The orientation of a rigid body in 3D space is described by three Euler angles. We use the following convention for Euler angles in our analysis: an initial azimuthal angle,  $\phi$ , about  $Z$ -axis, tilting angle,  $\theta$ , about the rotated  $y$ -axis, and pitching angle,  $\psi$ , about the rotated  $x$ -axis (figure 3). In the steady state, the pitching angle,  $\psi$  is very close to zero, therefore we only need to focus on  $\phi$  and  $\theta$  in this analysis. We obtain the azimuthal angle,  $\phi$ , by measuring the angle between the geometric principal axis of seed images in the bottom view and the  $X$ -axis.  $\phi = 0$  corresponds to the span-wise direction is along the  $X$ -axis. In order to compute the tilting angle,  $\theta$ , we measure the seed dimension along the span-wise direction,  $s$ , in the bottom view and normalize it with a measurement  $s_0$  from a static image in which the seed lies orthogonal to the camera direction. With the calibration data obtained in the previous section, the measurements are converted to physical units of length.  $\theta$  is inferred from the parallel projection formula,  $s = s_0 \cos \theta$ . Negative  $\theta$  means the seed tip lies above the root of the seed, which is the case when the seeds reach the steady state.

For dynamic calculations, it is necessary to track the position of the centre of mass in each image. To do so, we first need to determine the position of the centre of mass in the static frame,

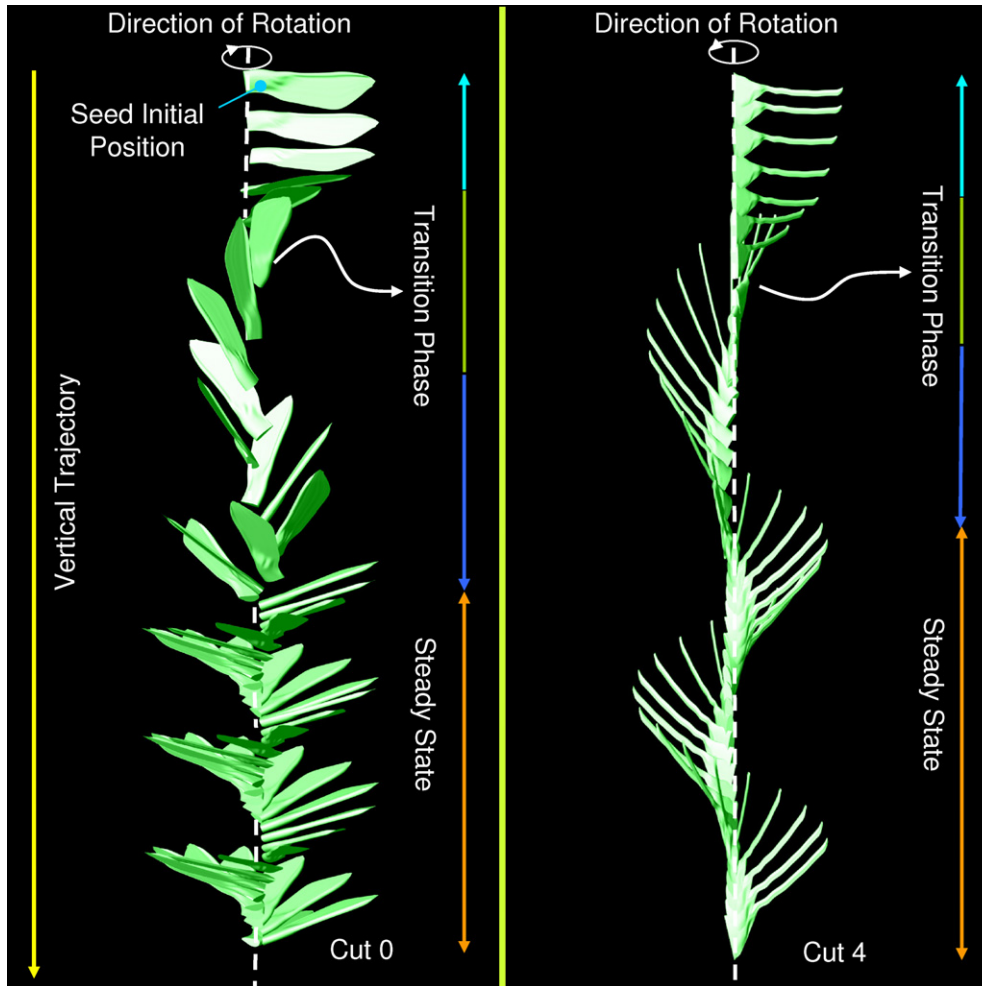


**Figure 2.** Side views of typical trajectories of a falling maple seed with intact and cut wings. The three-dimensional reconstructions are based on the side and bottom views recorded using a single high-speed camera. The seed is rendered using a computer-generated model. After releasing, the seed stays in transient phase which is subdivided into three phases and are shown by three different colors, for a while before reaching a steady-state helical motion.

and then identify this material point throughout the film. One way to determine the centre of mass of the seed is to balance the seed on a thin needle, but this turned out to be delicate because of the rounded surface of the nut. Instead, we calculate it based on the mass distribution. The seed can be decomposed roughly into three parts, the wing, the leading edge and the nut. Each has a fairly uniform mass density. Masses for these three parts are measured individually and based on that we compute the centre of mass,  $\vec{r}_{\text{com}} = \int \int \rho(x, y) \vec{r} d\vec{r}$ . To identify the centre of mass in each image, we define the centre of mass position in relation to the two other material points. In our case, we choose the two endpoints along the seed span,  $\vec{r}_1$  and  $\vec{r}_2$  which can be tracked. The instantaneous position of the centre of mass,  $\vec{r}_{\text{com}} = \vec{r}_1 + r_t(\vec{r}_2 - \vec{r}_1) + r_p \hat{Z} \times (\vec{r}_2 - \vec{r}_1)$  where  $r_t$  and  $r_p$  are related to displacements parallel and perpendicular to  $\vec{r}_2 - \vec{r}_1$ , which is calculated in each video frame.

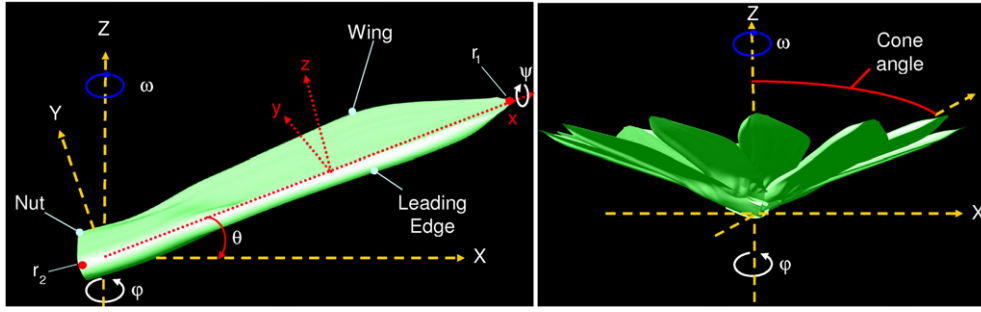


**Figure 3.** Geometrical configuration of the seed during its free-fall together with Euler angles and the symbols used. Dashed (yellow) lines show laboratory axes whereas dotted (red) lines show local seed axes.

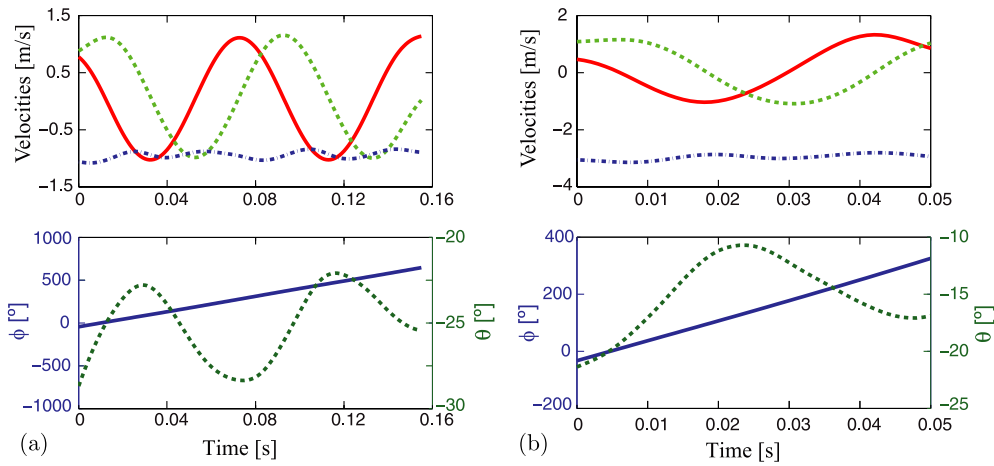


**Figure 4.** Steady-state kinematics. (a) wing cut0, (b) wing cut4. Top plots are 3D velocities,  $v_x$  (solid red line),  $v_y$  (dashed green), and  $v_z$  (dotted dashed blue). The bottom plots are two Euler angles,  $\phi$  (solid blue), and  $\theta$  (dashed green). The third Euler angle  $\psi$  is close to zero.

Figure 4 shows the time series of velocities and Euler angles for the two representative seeds, one for cut0 and the other for cut4. The numerical differentiations are computed through a robust locally weighted regression method [31]. In both cases, the terminal velocity remains approximately constant. The cut seed falls faster as expected. The azimuthal velocities,  $v_x$  and  $v_y$ , are two orthogonal components of the circular motion, which in two cases are surprisingly similar. There is a small drift associated with the tilt of the cone angle, which is estimated to be in the range  $6^\circ$ – $8^\circ$ .

Azimuthal angular velocity,  $\omega_\phi$ , is a constant in each falling for a given cut. The cut seed rotates almost 60% faster,  $\omega_\phi = 124.5 \text{ s}^{-1}$ , compared with the full seed  $\omega_\phi = 77.9 \text{ s}^{-1}$ . The oscillation in  $\theta(t)$  is due to the tilt of the cone axis. We estimate the cone angle as the complementary angle for averaged  $\theta$ . The cone angle is  $64.2^\circ$  for cut0 and  $73.6^\circ$  for cut4.

To examine the dependence of the falling kinematics on the shape of the seed, we carried out three sets of experiments with different seed alterations, by cutting separately the wing, the nut and the leading edge in small increments. The seed gyrates when (1) the leading edge is completely removed, (2) part of the nut is cut and (3) the wing is cut almost down to the

leading edge. Only when the nut is completely removed, the seed no longer gyrates, and falls erratically. Table 1 shows the comparison of the kinematics from these experiments. All cases exhibit qualitatively similar behaviour in the steady state. The variations are seen in the descending speed, the azimuthal angular velocity and the cone angle.

A curious result is that the cone angle remains relatively constant until an abrupt change to an erratic fall. Up to cut4, where the seed area is reduced almost by a factor of 3, the cone angle increases moderately from  $64.2^\circ$  to  $73.6^\circ$ . A sharp transition occurs at cut5, where the cone angle drops sharply even though the change in the seed shape is almost negligible.

#### 4. Initiation of gyration

The fact that the seeds with reduced wings also attain a helical path as the full seed suggests that while the aerodynamic force on the wing is effective in slowing down the descent, it has a relatively small effect on the initiation of the gyration. A close inspection of the film during the transition shows that the gyration occurs shortly after the release of the seed, well before the seed reaches a substantial velocity to produce a large aerodynamic force.

The initiation results from a subtle interplay between the rigid-body dynamics and the aerodynamics. Starting from rest, the seed tumbles about its span-wise direction, followed by a sharp tilt up towards the  $Z$ -axis. The tilted seed then proceeds to precess about the  $Z$ -axis and gradually settles into a steady helical motion with a larger cone angle. These three stages can be understood by considering the Euler's equations for the rigid-body dynamics subject to an aerodynamic torque due to the initial air damping  $\vec{\tau}$ ,

$$\begin{aligned} I_x \dot{\omega}_x &= (I_y - I_z) \omega_y \omega_z + \tau_x, \\ I_y \dot{\omega}_y &= (I_z - I_x) \omega_z \omega_x + \tau_y, \\ I_z \dot{\omega}_z &= (I_x - I_y) \omega_x \omega_y + \tau_z, \end{aligned}$$

where  $I_x < I_y < I_z$  are moments of inertia about the three principal axes.

Shortly after the release, the wing experiences a small air damping. An offset of the centre of pressure from the centre of mass causes the wing to rotate. Because the span-wise direction has the smallest moment of inertia, the turning motion manifests first along this axis, resulting in a tumble.

As the wing continues to fall, the centre of pressure remains close to the middle of the wing, and as a result the seed falls at an almost normal angle of attack. The centre of mass, on the other hand, is located near the nut. This creates a torque,  $\tau_y < 0$ , to tilt the seed up about the chord direction. The chord direction has an intermediate moment of inertia, and is inherently unstable. Due to this instability, the rotational energy is fed into the other two stable directions, which leads to an angular velocity around the  $Z$ -axis, and this initiates the helical motion.

As the angular moment gains in the two stable directions, the coupling between the two causes the seed to tilt down away from the  $Z$ -axis. To see this, we note that  $\omega_x$  and  $\omega_z$  always have the same sign. This results in a positive  $(I_z - I_x) \omega_z \omega_x$ , and when  $\omega_z \omega_x$  is sufficiently large, it overcomes the negative  $\tau_y$ , leading to  $\dot{\omega}_y > 0$ . Consequently, the seed tilts away from the  $Z$ -axis corresponding to a larger cone angle and eventually settling into a steady state.

#### 5. Conclusion

There are three essential ingredients that lead to the observed helical motion seen in maple seeds. The first is the asymmetric mass distribution of the seed, with the centre of mass far



away from the centroid of the seed. The second is the aerodynamic damping that initiates a tilt of the seed which eventually evolves into a helical motion due to the rigid-body dynamics. The third is the aerodynamic force in the steady state that balances the weight of the seed and the centrifugal force. The subtle coupling between the initial aerodynamic torque and the rigid-body dynamics distinguishes this case from all the other autorotational mechanisms discussed in the introduction.

## References

- [1] Augspurger C K 1986 Morphology and dispersal potential of wind-dispersed diaspores of neotropical trees *Am. J. Bot.* **73** 353–63
- [2] Horn H S, Nathan R and Kaplan S R 2001 Long-distance dispersal of tree seeds by wind *Ecol. Res.* **16** 877–85
- [3] Nathan R, Katul G G, Horn H S, Thomas S M, Oren R, Avissar R, Pacala S W and Levin S A 2002 Mechanisms of long-distance dispersal of seeds by wind *Nature* **418** 409–13
- [4] Norberg R A 1973 Autorotation, self-stability, and structure of single-winged fruits and seeds (samara) with comparative remarks on animal flight *Bio. Rev.* **48** 561–96
- [5] Augspurger C K and Hogan K P 1983 Wind dispersal of fruits with variable seed number in a tropical tree (*Lonchocarpus Pentaphyllus* Leguminosae) *Am. J. Bot.* **70** 1031–7
- [6] Greene D F and Johnson E A 1990 The aerodynamics of plumed seeds *Funct. Ecol.* **4** 117–25
- [7] Minami S and Azuma A 2003 Various flying modes of wind-dispersal seeds *J. Theor. Biol.* **225** 1–14
- [8] Nathan R 2006 Long-distance dispersal of plants *Science* **313** 786–8
- [9] Azuma A and Yasuda K 1989 Flight performance of rotary seeds *J. Theor. Biol.* **138** 23–54
- [10] Yasuda K and Azuma A 1997 The autorotation boundary in the flight of samaras *J. Theor. Biol.* **185** 313–20
- [11] Lentink D, Dickson W B, van Leeuwen J L and Dickinson M H 2009 Leading-edge vortices elevate lift of autorotating plant seeds *Science* **324** 1438–40
- [12] McCutchen C W 1977 The spinning rotation of ash and tulip tree samaras *Science* **197** 691–2
- [13] Lugt H J 1983 Autorotation *Annu. Rev. Fluid Mech.* **15** 123–47
- [14] Skews B W 1991 Autorotation of many-sided bodies in an airstream *Nature* **352** 512–3
- [15] Smith E H 1971 Autorotating wings: an experimental investigation *J. Fluid Mech.* **50** 513–34
- [16] Skews B W 1990 Autorotation of rectangular plates *J. Fluid Mech.* **217** 33–40
- [17] Maxwell J C 1854 On a particular case of the descent of a heavy body in a resisting medium *Camb. Dublin Math.* **9** 115–18
- [18] Riabouchinsky D P 1935 Thirty years of theoretical and experimental research in fluid mechanics *London: R. Aeronaut. Soc.* **77** 283–348
- [19] Dupleich P 1941 Rotation in free fall of rectangular wings of elongated shape *NACA Tech. Mem.* **1201** 1–99
- [20] Willmarth W W, Hawk N E and Harvey R L 1964 Unsteady motions of wakes of freely falling disks *Phys. Fluids* **7** 197–208
- [21] Viets H and Lee D A 1971 Motion of freely falling spheres at moderate Reynolds numbers *Am. Inst. Aeronaut. Astronaut.* **9** 2038–42
- [22] Field S B, Klaus M, Moore M G and Nori F 1997 Chaotic dynamics of falling disks *Nature* **388** 252–4
- [23] Belmonte A, Eisenberg H and Moses E 1998 From flutter to tumble: Inertial drag and Froude similarity in falling paper *Phys. Rev. Lett.* **81** 345–8
- [24] Mahadevan L, Ryu W S and Samuel A D T 1999 Tumbling cards *Phys. Fluids* **11** 1–3
- [25] Andersen A, Pesavento U and Wang Z J 2005 Unsteady aerodynamics of fluttering and tumbling plates *J. Fluid Mech.* **541** 65–90
- [26] Andersen A, Pesavento U and Wang Z J 2005 Analysis of transitions between fluttering, tumbling and steady descent of falling cards *J. Fluid Mech.* **541** 91–104
- [27] Jones M A and Shelley M J 2005 Falling cards *J. Fluid Mech.* **540** 393–425
- [28] Varshney K 2008 Unsteady dynamics of wind turbine wake, oscillating bubble and falling card *PhD Thesis* UMass Amherst, Paper AAI3372281
- [29] Zhong H, Chen S and Lee C 2011 Experimental study of freely falling thin disks: transition from planar zigzag to spiral *Phys. Fluids* **23** 011702
- [30] Ern P, Risso F, Fabre D and Magnaudet J 2012 Wake-induced oscillatory paths of bodies freely rising or falling in fluids *Annu. Rev. Fluid Mech.* **44** 97–121
- [31] Cleveland W S 1979 Robust locally weighted regression and smoothing scatterplots *J. Am. Stat. Assoc.* **74** 829–36